

Thermal conductivity and heat diffusion in the two-dimensional Hubbard model

Martin Ulaga,¹ Jernej Mravlje,¹ Peter Prelovšek,¹ and Jure Kokalj^{2,1}

¹*Jozef Stefan Institute, Jamova 39, 1000 Ljubljana, Slovenia*

²*University of Ljubljana, Faculty of Civil and Geodetic Engineering, Jamova 2, 1000 Ljubljana, Slovenia*

We study the electronic thermal conductivity κ_{el} and the thermal diffusion constant $D_{\text{Q,el}}$ in the square lattice Hubbard model using the finite-temperature Lanczos method. We exploit the Nernst-Einstein relation for thermal transport and interpret the strong non-monotonous temperature dependence of κ_{el} in terms of that of $D_{\text{Q,el}}$ and the electronic specific heat c_{el} . We present also the results for the Heisenberg model on a square lattice and ladder geometries. We study the effects of doping and consider the doped case also with the dynamical mean-field theory. We show that κ_{el} is below the corresponding Mott-Ioffe-Regel value in almost all calculated regimes, while the mean free path is typically above or close to lattice spacing. We discuss the opposite effect of quasi-particle renormalization on charge and heat diffusion constants. We calculate the Lorenz ratio and show that it differs from the Sommerfeld value. We discuss our results in relation to experiments on cuprates. Additionally, we calculate the thermal conductivity of overdoped cuprates within the anisotropic marginal Fermi liquid phenomenological approach.

I. INTRODUCTION

Thermal conductivity is a powerful probe of correlated electrons which, e.g., allowed detection of the breakdown of the Fermi-liquid theory in cuprate superconductor [1], observing highly mobile excitations in organic spin liquid [2] and determining the absence of quasiparticles in electronic fluid of vanadium dioxide [3]. Despite this, thermal conductivity receives less attention than the charge conductivity, which was recently measured also in optical lattices [4], and was explored theoretically with precise numerical simulations both in the high-temperature bad metal [4–8] and lower temperature strange metal regime [9].

Both cold atom measurements [4] and theoretical discussions of transport properties employ the Nernst-Einstein relation that expresses the conductivity $\sigma_c = \chi_c D_c$ in terms of the charge susceptibility χ_c and the charge diffusion constant D_c . At high temperatures the temperature dependence of σ_c is dominated by χ_c [4–6] and one can understand the appearance of bad-metallicity (conductivity below the Mott-Ioffe-Regel value [10]) in terms of decreasing χ_c and saturated, temperature independent D_c . Similarly, one can express the spin conductivity $\sigma_s = \chi_s D_s$ (with χ_s being the uniform spin susceptibility and D_s being the spin diffusion constant). This was used in a study of spin transport in cold atoms [11]. The spin diffusion constant has a non-monotonic T -dependence and reaches values below the lower limit of charge diffusion. This occurs because the velocity is reduced from a value given by hopping t to a lower one given by the (lower energy) Heisenberg exchange J [11, 12].

One can also discuss the thermal conductivity along the lines of the corresponding Nernst-Einstein relation $\kappa = c D_{\text{Q}}$ (with c being the specific heat and D_{Q} the heat diffusion constant). In contrast to the case of

charge conductivity, κ , c and D_{Q} can all be independently measured [13–15]. One could thus hope for better characterization of the electronic transport, but $\kappa = \kappa_{\text{ph}} + \kappa_{\text{el}}$ has both electronic and phononic contributions and separating them is not straightforward. One typically resorts to estimating electronic contribution κ_{el} via the Wiedemann-Franz law, which, however is often violated [3, 16–19]. The difficulty to unambiguously identify the two contributions can be illustrated in the case of the normal state in cuprates, where one can find quite diverse claims: (i) κ_{el} represents about a half of the total κ [20, 21] or (ii) a very small portion of total κ [14, 22] (iii) which contrasts with a surprisingly large magnonic contribution found in Ref. 23, and (iv) total κ showing the same in-plane anisotropy as σ_c , suggesting it has an electronic origin [13]. Recent studies discuss the phononic part κ_{ph} in terms of a Planckian relaxation rate [14, 24], but they could still be affected by the uncertainties in the subtraction of the electronic part.

Is the behavior of κ_{el} better characterized at least within theory? Thermal transport was broadly studied in one-dimensional systems in part due to much larger values of κ originating in long mean free paths and proximity to integrability [25–28]. Results for dimension $d > 1$ are however scarce. The Hubbard model in 2 dimensions was very recently studied with a determinant quantum Monte Carlo investigation of the Mott insulator [29] and with a weak coupling approach [30], but no other results exist. We are unaware of any calculation of thermal conductivity even for the more basic 2d Heisenberg model. It is important to have robust numerical results for κ_{el} not only to address the fundamental questions, e.g., asymptotic behavior of the diffusion constant and relaxation rates, but also to help interpreting the experiments.

In this work we study the thermal conductivity and

the heat diffusion constant in the square lattice Hubbard model with the finite temperature Lanczos method (FTLM). We study also the Heisenberg model both on square lattice and ladder geometries. Our FTLM calculations are limited to $T \gtrsim J/2$ and thus map out the high temperature regime of the phase diagram and are directly relevant for the cold atom experiments [4, 11, 31, 32]. There the density, spin density and energy density relaxations are affected also by a thermal conduction either directly or via mixed, e.g., thermoelectric effects [33]. For materials, the experimental temperatures are usually lower. To discuss this regime we thus resort to a phenomenological spin-wave model, qualitative aspects of the dynamical mean field theory (DMFT) results, and the phenomenological anisotropic marginal Fermi liquid model (AMFL). The latter captures various aspects of overdoped cuprates [34, 35]. We discuss our results for the Mott-insulating and doped cases in relation to experiments on cuprates.

The paper is structured as follows. In Sec. II we present models and methods. We show the results for the Mott insulating state with strongly nonmonotonic behavior of κ_{el} in Sec. III, where we also discuss the difference between the Hubbard and Heisenberg model results. The effect of doping is presented in Sec. IV and the violation of the Wiedemann-Franz law is discussed in Sec. V. In Sec. VI, our results are discussed in relation to experiments on cuprates for undoped and doped regime. We summarize our findings in Sec. VII. Appendix A contains technical details of FTLM calculations. We discuss cluster shape dependence of the results in Appendix B, frequency dependence of conductivity in Appendix C, vertex corrections in Appendix D, the quasiparticle regime in Appendix E and the AMFL phenomenology for overdoped cuprates in Appendix F.

II. MODEL AND METHOD

We consider the Hubbard model on a square lattice,

$$H = -t \sum_{\langle i,j \rangle, s} c_{i,s}^\dagger c_{j,s} + U \sum_i n_{i,\uparrow} n_{i,\downarrow}, \quad (1)$$

where $c_{i,s}^\dagger/c_{i,s}$ create/annihilate an electron with spin s (either \uparrow or \downarrow) at the lattice site i . The hopping amplitude between the nearest neighbors is t . We further set $\hbar = k_B = e = 1$. We denote the lattice parameter with a .

We investigate the model with FTLM [36–38] on a cluster with size $N = 4 \times 4$. To reduce the finite-size effects that appear at low T , we employ averaging over twisted boundary conditions and use the grand canonical ensemble. We do not show results in the low T regime where our estimated uncertainty due to finite size effects and spectra broadening exceeds 20%. We

also perform FTLM calculations on the square lattice Heisenberg model with up to 32 sites and additionally on 2 leg and 3 leg ladders. For the Hubbard model away from half filling, we additionally compare our results with single-site DMFT calculations, obtained with NRG-Ljubljana [39, 40] as the impurity solver.

The electronic thermal conductivity is calculated as

$$\kappa_{\text{el}} = \frac{L_{22}}{T} - \frac{L_{21}^2}{TL_{11}}, \quad (2)$$

where L_{ij} represent corresponding conductivities with $L_{11} = \sigma_{n,n} = \sigma_c$, $L_{12} = L_{21} = \sigma_{Q,n}$ and $L_{22} = \sigma_{Q,Q}$. Within FTLM [36], these are obtained as the frequency $\omega = 0$ value of the dynamical conductivities related to the current-current correlation functions $\sigma_{A,B}(\omega) = \text{Im}\chi_{A,B}(\omega)/\omega$ while in DMFT they are calculated with the bubble approximation. The heat current j_Q is given by the energy j_E and particle j_n currents, $j_Q = j_E - \mu j_n$. Within the Heisenberg model κ_{el} is calculated as $\kappa_{\text{el}} = \sigma_{E,E}/T$. More details on the calculations are given in Appendix A.

III. MOTT INSULATOR

We show κ_{el} for $U = 5t$, $10t$ and $20t$ in the half-filled ($n = 1$, doping $p = 1 - n = 0$) Mott-insulating case in Fig. 1a. The most prominent feature is the non-monotonic T dependence with a large maximum at high T , e.g., at $T \sim 2t$ for $U = 10t$. This maximum can be understood via the Nernst-Einstein relation $\kappa_{\text{el}} = c_{\text{el}} D_{Q,\text{el}}$ in terms of a maximum in the electronic specific heat c_{el} [41]. This maximum is shown in Fig. 1b and is the high- T maximum in c_{el} (opposed to low- T maximum in c_{el} at $T < t$) and originates in the increase of the entropy from the spin (Heisenberg) value $\ln(2)$ towards a full charge activated value $\ln(4)$ via the thermal activation of mobile doublons and holons [42] across the charge gap Δ_c [38, 43]. It moves to higher T with increasing U (see Figs. 1a,b). The maximum in κ_{el} at high T is therefore a consequence of the new heat conduction channel via particles, doublons and holons.

At lower T , e.g., $T < 2t$ for $U = 10t$, κ_{el} decreases faster with decreasing T than c_{el} (see Figs. 1a,b). This is due to strong decrease of the electronic heat diffusion constant $D_{Q,\text{el}}$ (see Fig. 1c) and indicates a crossover from particle dominated to spin (wave) dominated heat transport at lower T and the accompanying strong decrease of the average velocity v determining the diffusion constant $D = vl/2$ [12]. The velocity v decreases from the order of $v \sim ta$ to the order of $v \sim Ja$. Here $J = 4t^2/U$ is the exchange coupling [44] and l is the mean free path. $D_{Q,\text{el}}$ is calculated via the Nernst-Einstein relation $D_{Q,\text{el}} = \kappa_{\text{el}}/c_{\text{el}}$.

At even lower $T \sim J$, c_{el} shows a peak due to spin excitations [36, 38, 43]. For large U this peak can be

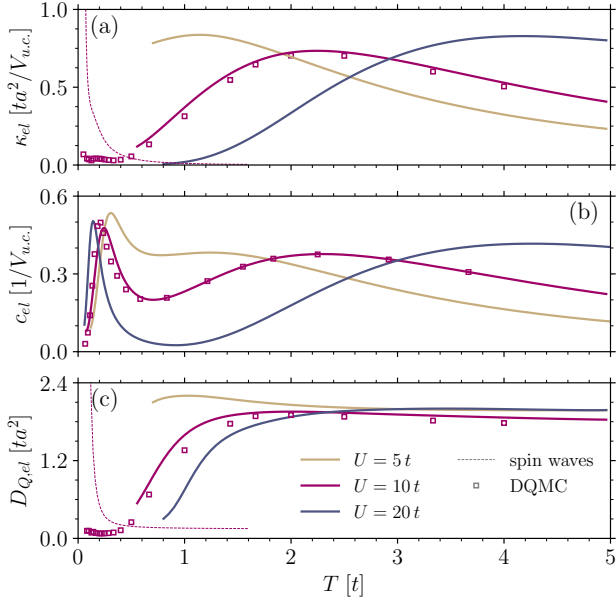


FIG. 1. The electronic thermal conductivity κ_{el} , specific heat c_{el} , and thermal diffusion constant $D_{Q,el}$ for a half-filled (doping $p = 0$) Hubbard model with $U = 5t, 10t$ and $20t$. The full thick lines are FTLM results and the squares are DQMC data taken from Ref. 29. The thin dashed lines in a) and c) denoted “spin waves” are the phenomenological approximation for the spin (Heisenberg) part and are obtained as explained in the main text, fixing $J = 4t^2/U = 0.4t$.

well described with the Heisenberg model as is shown in Fig. 2b. Our FTLM Heisenberg results on 32 sites for c_{el} agree well with the results from Refs. 45 and 46 and also reasonably with those from Refs. 47 and 48, where a peak occurs at a slightly lower T . Whether this peak in c_{el} manifests as a peak in κ_{el} depends on the strength of the T dependence of $D_{Q,el}$. If $D_{Q,el}$ increased strongly with decreasing T , the peak in c_{el} would appear only as a shoulder in κ_{el} .

To explore lower $T \lesssim J$ behavior, we calculate κ_{el} in the Heisenberg model using FTLM. The results are shown in Fig. 2 next to the Hubbard model results for $U = 10t$. The Heisenberg model κ_{el} monotonically increases with decreasing T (Fig. 2a). This increase becomes less steep at lowest T that reach below the ones corresponding to the low- T peak in c_{el} . The diffusion constant is shown on Fig. 2c. It is essentially temperature-independent above $T \sim J$, but increases below it. We studied additional cluster sizes and shapes with FTLM and report the results in Appendix B. Finite clusters indicate a peak in κ_{el} corresponding to the peak in c_{el} , but the finite size effects are significant there: with increasing cluster size κ_{el} is still increasing.

The Heisenberg model results reach values significantly above the DQMC Hubbard model results for $T < J$. We do not understand this discrepancy. One could at-

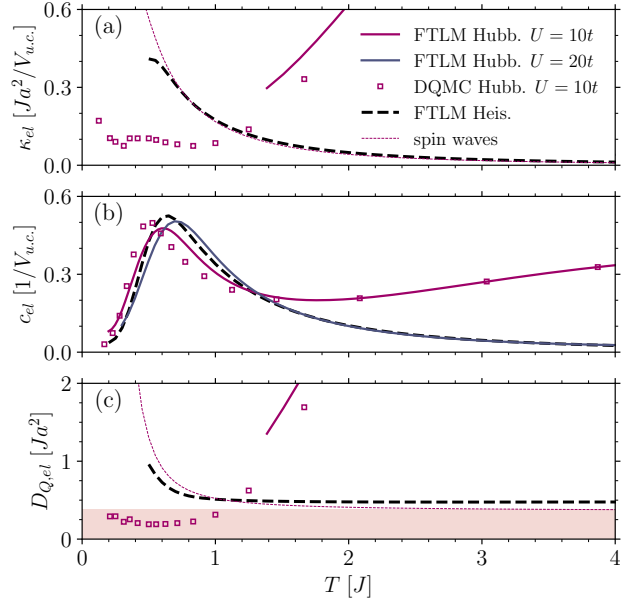


FIG. 2. κ_{el} , c_{el} and $D_{Q,el}$ calculated with FTLM and DQMC compared to Heisenberg model FTLM ($N = 32$) results. The results are shown in units of exchange coupling $J = 4t^2/U$. Results are compared also to the “spin waves” approximation (thin dashed line) explained in the main text. The shaded area indicates the region of spin MIR limit violation. DQMC data are taken from Ref. 29.

tribute this to the difficulties associated with analytical continuation in DQMC but note that the agreement between DQMC and FTLM results for the Hubbard model at higher T is good (see also Appendix C). The other option could be the higher order corrections in t/U expansion of the Hubbard model.

We compare our numerical results also with a phenomenological model. For this, we take c_{el} from FTLM Heisenberg model results and approximate the mean free path by the spin-spin correlation length ξ from renormalization group calculations [49, 50]

$$l = \sqrt{[C_\xi a \exp(2\pi\rho_s/T)/(1 + 1/(2\pi\rho_s/T))]^2 + a^2}. \quad (3)$$

ξ is modified to approach $l(T \rightarrow \infty) \rightarrow a$ and obtained with $C_\xi = 0.5$ and $\rho_s = 0.15J$ and T in units of J . We approximate the velocity v with the kinetic magnon approximation [51], which gives $v \sim 0.72Ja$ at highest T and interpolates to $v \sim 1.4Ja$ at low T [12, 50, 52]. From this, we obtain $D_{Q,el} = vl/2$ and $\kappa_{el} = c_{el}D_{Q,el}$ and show them in Fig. 1 and 2 with thin dashed lines denoted “spin waves”. The obtained diffusion constant (taking $l = a$) agrees with the known limiting value of the spin diffusion constant $D_s \sim 0.4Ja^2$ in the Heisenberg model at high T [53]. The agreement between the DQMC result and this spin wave estimate in Fig. 2a is poor.

On the other hand, the T dependence of the spin wave estimate and Heisenberg model results agree qualitatively. $D_{Q,\text{el}}$ in the Heisenberg model at high T is close to the spin-wave estimate (see Fig. 2c). At lower $T < J$ one expects $D_{Q,\text{el}}$ to increase (and diverge with $T \rightarrow 0$) due to increased (diverging) l . It is also expected that the Heisenberg $D_{Q,\text{el}}$ is smaller than the spin wave estimate as observed in Fig. 2c. Namely, one expects $l \lesssim \xi$ since spin waves are expected to scatter at the antiferromagnetic domain walls separated effectively by ξ .

IV. DOPED MOTT INSULATOR

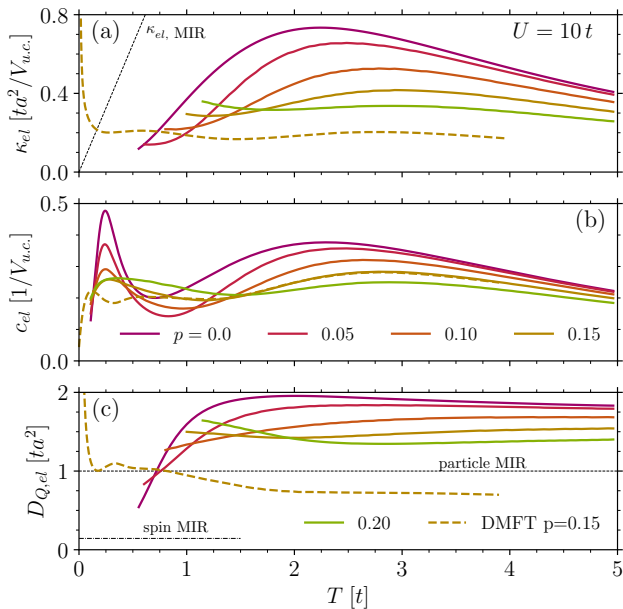


FIG. 3. The temperature dependence of κ_{el} (a), c_{el} (b), and $D_{Q,\text{el}}$ (c) for several hole dopings p and for $U = 10t$ as obtained with FTLM. DMFT results for $p = 0.15$ are also shown. Characteristic MIR limits are indicated in (a) and (c) (see text).

We now consider the effect of doping. We show κ_{el} for several hole dopings p and for $U = 10t$ in Fig. 3a. With increasing p the high- T peak at $T \sim 2.5t$ becomes less pronounced, due to suppressed c_{el} (Fig. 3b) and lower release of entropy via thermal activation of holons and doublons. In comparison to the Mott insulating case, κ_{el} at $T \lesssim t$ is increased due to charge conduction. The increase at low- T for larger dopings indicate the onset of coherence.

A. Mott-Ioffe-Regel limit for κ_{el}

Like for the case of charge conductivity σ_c , we can introduce the MIR value that indicates the minimal conduction within the Boltzmann estimate by setting $l \sim a$. In 2d it is given by [54]

$$\kappa_{\text{el,MIR}} = \frac{\pi^2 T}{3} \frac{\sqrt{n} a^2}{\sqrt{2\pi} V_{\text{u.c.}}} \quad (4)$$

With our units and filling $n \sim 1$ one obtains $\kappa_{\text{el,MIR}} \sim 1.3Ta^2/V_{\text{u.c.}}$. This value is indicated in Fig. 3a and our κ_{el} is well below it. It has been shown, that violations of the MIR limit for the charge conductivity [4–6] (and spin conductivity [12]) originate in strongly suppressed static charge susceptibility (or spin susceptibility), while the diffusion constant and mean free path still correspond to $l \gtrsim a$. Is this the case also for κ_{el} ?

In Fig. 3c we compare the calculated $D_{Q,\text{el}}$ with the corresponding MIR value $D_{Q,\text{el,MIR}} = va/2$. The expected velocity in the doped case is the quasiparticle velocity, which we approximate with $v \sim 2ta$. This leads to $D_{Q,\text{el,MIR}} \sim ta^2$. For almost all parameter regimes we observe $D_{Q,\text{el}} > D_{Q,\text{el,MIR}}$ and $l \gtrsim a$. At lowest T and half-filling ($p = 0$) one expects lower limiting values as the heat conductance is dominated by spins with lower velocity $v \sim Ja$. If one uses the spin-wave velocity $v \sim 0.72Ja$ [51] one obtains the lower bound $D_{Q,\text{el,MIR,spin}} \sim 0.36Ja^2$, namely $D_{Q,\text{el,MIR,spin}} \sim 0.14ta^2$ for $U = 10t$. This value is indicated in Fig. 3c and $D_{Q,\text{el}}$ for $p = 0$ is above it and only approaches it with lowering T . This is also shown in Fig. 2c together with the Heisenberg model results, which saturates closely to the MIR value (indicated by shading).

On the other hand, the DQMC results at the lowest T are below the bound and the FTLM results for low doping ($p = 0.05$) at the lowest T cross the $D_{Q,\text{el,MIR}} \sim ta^2$ (see Fig. 3c). Reconciliation of this in terms of a possible deconstruction $\kappa_{\text{el}} = \kappa_{\text{spin}} + \kappa_{\text{particle}}$ or with effectively decreased velocity from the order of $v \sim ta$ to $v \sim Ja$ remains a subject for future work.

Let us also note that as $T \rightarrow 0$ the mean free path is expected to diverge, leading to diverging $D_{Q,\text{el}}(T \rightarrow 0) \rightarrow \infty$ within the Hubbard model. Therefore, $D_{Q,\text{el}}$ has a non-monotonic T dependence.

To qualitatively explore the behavior at lower T , we performed also DMFT calculations for $p = 0.15$ and show the results in Fig. 3. The DMFT results display a divergence of κ_{el} and $D_{Q,\text{el}}$ as $T \rightarrow 0$. This rapid growth occurs below $T \sim 0.1t$ due to low coherence temperature. Remarkably the upturn appears at T where $\kappa_{\text{el}} \sim \kappa_{\text{el,MIR}}$ (see Fig. 3a). Similar behavior is observed for charge transport [55].

B. Comparison of heat and charge diffusion

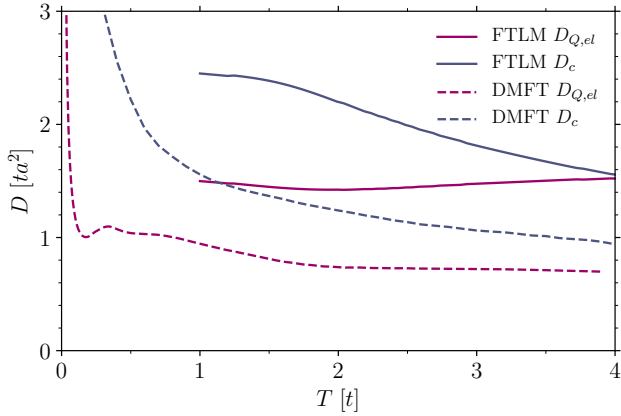


FIG. 4. Comparison of heat and charge diffusion constants $D_{Q,el}$ and D_c as obtained by FTLM and DMFT. $U = 10t$, $p = 0.15$.

For the doped case, it is interesting to compare heat $D_{Q,el}$ and charge D_c diffusion constants. This is shown in Fig. 4 and one can see that $D_{Q,el}$ and D_c behave differently. The thermal diffusion constant depends on temperature more weakly. One can also see that $D_{Q,el}$ is smaller than D_c for $T \lesssim 4t$. The heat transport seems less coherent at lower T . Similar trends as indicated by FTLM results continue to higher T , where at very high T $D_{Q,el} \sim 1.6ta^2$ and is larger than $D_c \sim ta^2$. This difference is currently not understood.

We also show the DMFT result and find that $D_{Q,el}$ and D_c differ even at low T . The difference between FTLM and DMFT result can be attributed to vertex corrections. We discuss this in more detail in Appendix D, where we also show the frequency dependent $\kappa_{el}(\omega)$ which has a peak at $\omega \sim U/2$ which is not seen in $\sigma_c(\omega)$.

C. Low T metallic regime

The lowest T behavior with diverging κ_{el} and $D_{Q,el}$, can be described within quasiparticle picture. We start with the bubble formulas for both κ_{el} and σ_c and with certain approximations (Appendix E) rewrite them in terms of the quasiparticle properties. Using Eqs. E7 and E8 for κ_{el} and σ_c with known approximations [38, 56]

$$c_{el} = \frac{\pi^2}{3} \frac{g_0(\epsilon_F)}{z} T, \quad (5)$$

$$\chi_c = z g_0(\epsilon_F), \quad (6)$$

one obtains via the Nernst-Einstein relation

$$D_{Q,el} \simeq z \frac{v_{0,F}^2}{-4\Sigma''(0)}, \quad (7)$$

$$D_c \simeq z^{-1} \frac{v_{0,F}^2}{-4\Sigma''(0)}. \quad (8)$$

Here $g_0(\epsilon_F)$ is a bare band density of states at Fermi energy, $v_{0,F}$ is bare Fermi velocity, $\Sigma''(0)$ is imaginary part of self energy at $\omega = 0$ and $z = 1/(1 - \partial_\omega \Sigma'(\omega)|_{\omega=0})$ is the quasiparticle renormalization.

$D_{Q,el}$ is decreased from the bare non-renormalized value $D_0 = v_{0,F}^2/[-4\Sigma''(0)]$ to $D_{Q,el} = zD_0$ with $z < 1$ while $D_c = D_0/z$ is increased. Therefore in the Fermi liquid regime the two diffusion constants differ by a factor of z^2 and therefore easily by an order of magnitude. The question on renormalization effect for diffusion was posed already in Ref. 57. Note that only $D_{Q,el}$ can be expressed in terms of the quasiparticle velocity $v_{qp} = zv_{0,F}$ and life time $\tau_{qp} = [-2z\Sigma''(0)]^{-1}$ as $D_{Q,el} = v_{qp}^2 \tau_{qp}/2$, but not D_c .

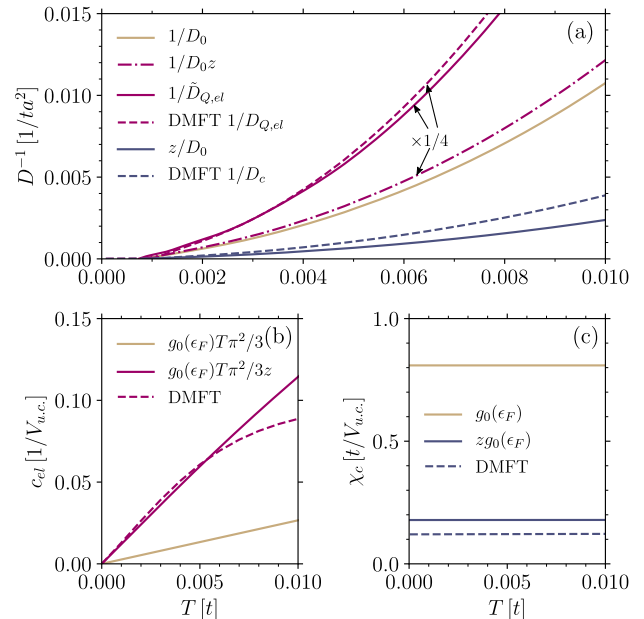


FIG. 5. DMFT results in the low- T Fermi liquid regime compared with simplified expressions (see main text) in terms of a quasi-particle properties. (a) Comparison for diffusion constants. All estimates for $D_{Q,el}$ (purple) are divided by 4 for compactness and clarity. (b) Comparison of c_{el} with Sommerfeld expression with non-renormalized and renormalized density of states. (c) Comparisons of DMFT χ_c with $g_0(\epsilon_F)$ and renormalized value $z g_0(\epsilon_F)$. $U = 10t$, $p = 0.15$, $z \approx 0.22$.

We illustrate these considerations with the DMFT results [58] shown in Fig. 5. D_c agrees better with D_0/z

than with D_0 and zD_0 is closer to DMFT $D_{Q,el} = \kappa_{el}/c_{el}$ than D_0 . Some mismatch persists in the latter, originating in our oversimplification of assuming a constant $\Sigma''(\omega) \sim \Sigma''(0)$ (see Appendix D). $\Sigma''(\omega)$ can have notable ω dependence (e.g., $\Sigma''(\omega) \propto \omega^2$ in FL) and the factor $(-\frac{\partial n_F}{\partial \omega})\omega^2$ in Eq. E5 filters out finite frequencies. Explicitly, frequencies at around $|\omega| \sim 3T$ are mainly included. We therefore compare DMFT $D_{Q,el}$ also with $\tilde{D}_{Q,el} = zv_{0,F}^2/[-4\Sigma''(\omega = 3T)]$ [59] and find good agreement. For completeness, Fig. 5(b,c) also show that c_{el} and χ_c are well approximated with renormalized values given in Eqs. 5 and 6.

V. THE WIEDEMANN-FRANZ LAW

The above discussion of different T dependence of $D_{Q,el}$ and D_c suggests a possible violation of the Wiedemann-Franz (WF) law and the deviation of the Lorenz ratio

$$\mathcal{L} = \frac{\kappa_{el}}{T\sigma_c} \quad (9)$$

from the Sommerfeld value $\pi^2/3$. In Fig. 6 we show the calculated Lorenz ratio and observe in the whole calculated regime a clear deviation from the Sommerfeld value. In addition, we find a strong T dependence which is also non-monotonic for small p .

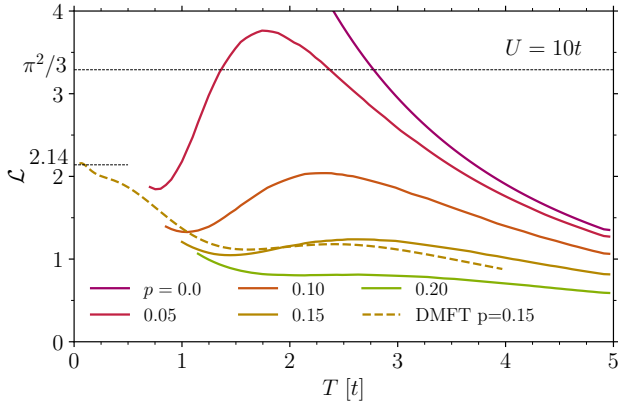


FIG. 6. Lorenz ratio vs. T for several hole dopings calculated with FTLM. DMFT result for $p = 0.15$ is shown. A low- T pure Fermi liquid result $\mathcal{L} = 2.14$ is also shown [60].

We now discuss the various violations of the WF law. In the high T limit this violation follows trivially as $L_{ij} \propto 1/T$, leading to $\kappa_{el} \propto 1/T^2$ and $\sigma_c \propto 1/T$ [61]. This gives $\mathcal{L} \propto 1/T^2$ in the high T limit [6], which is observed also in our results. The WF law is also violated for zero doping at low T , since κ_{el} has a nonzero spin contribution while σ_c is exponentially suppressed. \mathcal{L} is

therefore expected to exponentially diverge as $T \rightarrow 0$, which is seen in Fig. 6.

In the doped case at intermediate T , \mathcal{L} is not well described by the Sommerfeld value either. One finds a non-monotonic T dependence with a maximum. This maximum is most pronounced for low $p \sim 0.05$, where \mathcal{L} at higher T is most similar to the undoped case. It is therefore possible to ascribe the maximum at $T \sim 2t$ to the spin contribution. Even in the Fermi-liquid regime $\mathcal{L} \sim 2.14$ [60] due to κ_{el} taking into account higher ω scattering rate, while σ_c is affected more by a $\omega \sim 0$ scattering rate. See Fig. 6 and section IV C.

\mathcal{L} equals $\pi^2/3$ only for ω -independent scattering rates (see Appendix D), which appears, e.g., in the elastic impurity dominated scattering and when vertex correction are negligible. This is demonstrated in Fig. 13 with the AMFL model results at low T . The DQMC results for \mathcal{L} in the Hubbard model are discussed in Ref. [62].

It is interesting to note that the DMFT result for \mathcal{L} approximately agrees with the FTLM result as seen in Fig. 6 while the conductivities κ_{el} and σ_c differ even by a factor close to 2 as shown in the Appendix D. This suggests that in the DMFT missing vertex corrections [7, 8] in κ_{el} and σ_c almost cancel when calculating \mathcal{L} .

VI. DISCUSSION OF EXPERIMENTS

The purpose of this section is to discuss our results in terms of measurements on cuprates. The FTLM results do not reach sufficiently low temperatures for a direct comparison but the approximative extrapolations (spin-wave estimate in the undoped case and the DMFT in the doped case) do. For the doped case we also present the results of the phenomenological anisotropic marginal Fermi liquid model and compare them to the measurements on overdoped cuprates in Appendix F.

A. Mott-insulating LCO

Fig. 7 displays our results next to the measured κ_{el} [23] in La_2CuO_4 (LCO), the parent Mott-insulating cuprate compound [63]. The measured data represent the magnonic (spin) contribution to κ as the contribution from phonons was subtracted. A prominent feature in the measured data is the peak at $T \sim 300$ K. It appears due to the saturation of l at low T (a finite impurity concentration) and decreasing $c_{el} \rightarrow 0$ as $T \rightarrow 0$. On the high temperature side, measured κ_{el} drops due to decreasing l .

Our FTLM data are reliable only at higher T and the results for the $U = 10t$ Hubbard model still decrease with decreasing T . The Heisenberg model result at lowest

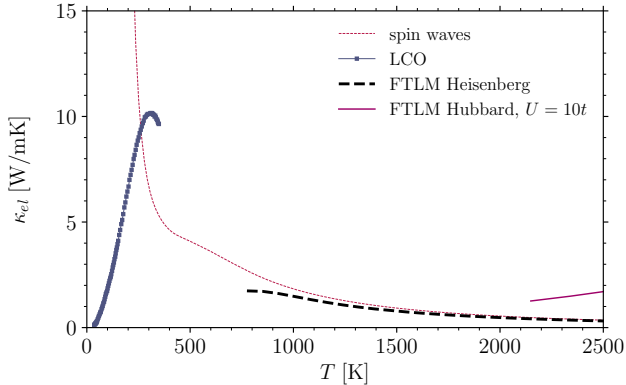


FIG. 7. Experimental κ_{el} for La_2CuO_4 taken from Ref. 23 plotted next to theoretical estimates.

$T \sim 800$ K is $\kappa_{el} \sim 2$ W/mK. The measured κ_{el} reaches ~ 10 W/mK at $T \sim 400$ K. To account for this increase, l has to increase by a factor of ~ 20 (note that c_{el} is already decreasing). Such an increase is not observed in the DQMC Hubbard model results (see Fig. 2a).

Also instructive is to compare the data with the spin-wave estimate. Because in this we do not include the saturation of l at low T due to imperfections, the spin-wave κ_{el} diverges at low T . The growth is moderate around 500 K but becomes more rapid at lower T due to a rapidly increasing l , e.g. $l \sim 50a$ at 300 K. Interestingly, the spin-wave result is still lower than the experimental value at this T .

B. The doped Mott insulator YBCO

In Fig. 8 we compare our κ_{el} results with the data for doped $\text{YBa}_2\text{Cu}_3\text{O}_{7-y}$ (YBCO) as reported in Ref. 64. Note that the measured data are available only at $T < 300$ K while the FTLM results are reliable only at $T > 2500$ K [65]. We plot also the DMFT result, which agrees with experimental data surprisingly well.

The key aspect of the data is that the values of κ_{el} in FTLM at 3000 K are quite close to the measured ones at 300 K and that DMFT indicates a T independent κ_{el} . We expect that the actual κ_{el} is higher than the DMFT one. The FTLM result on κ_{el} for doping $p = 0.15$ shows a rather weak T dependence in Fig. 8, which is reminiscent of experimental behavior [64, 66], albeit at significantly higher T .

It is worth mentioning that linear-in- T c_{el} and linear-in- T electrical resistivity due to scattering rate (e.g., $D \propto 1/T$ in a bad or strange metal) can lead to T -independent or close to constant κ_{el} , at least for Lorenz ratio with weak T dependence.

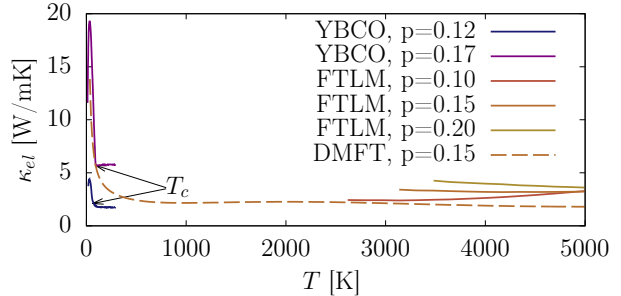


FIG. 8. Comparison of measured κ_{el} for doped cuprate $\text{YBa}_2\text{Cu}_3\text{O}_{7-y}$ with Hubbard model results for $U=10t$. κ_{el} are taken from Ref. 64 and are obtained by subtracting the estimated κ_{ph} . The data are for samples with $y = 6.68$ and $y = 6.93$, which correspond to dopings $p = 0.12$ and $p = 0.17$, respectively. Above T_c the experimental κ_{el} shows weak T dependence and similar magnitude as the DMFT and FTLM results at much higher $T \sim 3000$ K.

We note that the measured data show a strong increase below T_c . This is a superconducting effect and it has been suggested that it appears due to the increased coherence of non-superconducting electrons [67]. The low- T increase of DMFT results is not related to superconductivity, but originates in the increased coherence and longer l . However, such increase could be suppressed or restricted to lower T by spin, charge or order parameter phase fluctuations, which are not included in DMFT. These could explain the weak T dependence measured in the normal state.

Let us note in passing that D_Q was measured for several cuprates [13, 14] to have typical values of 0.02 cm²/s at high T ($\sim 300 - 600$ K). Taking the estimated lower bound on electronic thermal diffusion $D_{Q,el,MIR} = ta^2 \sim 0.7$ cm²/s, it is evident that the measured D_Q is smaller by an order of magnitude. This is due to the heat transfer being dominated by phonons, which have orders of magnitude smaller velocity than electrons.

It is also interesting to note that κ_{el} in the Mott insulator [23] has values around 10 W/mK at 300 K (Fig. 7), which is an order of magnitude larger than in the low doping metallic phase [13, 20, 64], where $\kappa \approx 1$ W/mK (Fig. 8). The magnonic part of c_{el} ($\propto T^2$) is smaller than in the doped case ($\propto T$, see also lowest T results in Fig. 6b) and the spin-wave velocity ($v \sim Ja$) is smaller than the particle velocity ($v \sim ta$). This indicates that quasiparticles have orders of magnitude smaller l than spin-waves and that their transport is at low doping significantly less coherent.

This is also in accord with strongly underdoped YBCO ($y = 6.34$) being taken in Ref. 64 as a case with smallest κ_{el} . We discuss the experimental Lorenz ratio for YBCO in Appendix F 2, where we compare it to the AMFL model results and discuss the relation of its tem-

perature dependence to the frequency dependence of the scattering rate.

VII. CONCLUSIONS

We studied κ_{el} and $D_{\text{Q,el}}$ with numerical calculations of square lattice Hubbard and Heisenberg models and further with phenomenological models.

In the Mott-insulating phase κ_{el} is nonmonotonic and has three features. It has a high- T peak related to a peak in c_{el} due to charge excitations. c_{el} has another peak at $T \sim 0.6J$ and drops at lower T due to the quenching of the spin-entropy. This happens at T below that accessible to us in the numerical calculations of transport. However in our spin-wave phenomenological estimate the dependence of c_{el} at $T \sim J$ does not lead to a peak in κ_{el} , only a shoulder, while the situation in the Hubbard and Heisenberg models remains unsettled. At even lower T , κ_{el} peaks (diverges in a pure model) due to increased l . The Hubbard model κ_{el} and $D_{\text{Q,el}}$ approach the Heisenberg model results with decreasing T . At lower $T < J$, the difference between the Heisenberg model results and DQMC Hubbard results deserves further study.

We introduced a MIR value for thermal conductivity and found that at higher T , κ_{el} is below it, thus violating the naïve bound. Conversely, the calculated thermal diffusion $D_{\text{Q,el}}$ has values that correspond to $l \gtrsim a$ (except for smallest dopings that can be perhaps understood in terms of suppressed velocity). The thermal transport thus behaves analogously to the charge transport in this respect. The analogy is however incomplete. We compared the temperature dependences of $D_{\text{Q,el}}$ and D_c and found they behave differently: in the intermediate temperature regime $D_{\text{Q,el}}$ has a more incoherent behavior and less temperature dependence than D_c . In the well defined quasiparticle regime $D_{\text{Q,el}}$ and D_c behave differently upon renormalization and differ by a factor of z^2 . The renormalization in cuprates is typically $1/z = 3-4$, thus $D_{\text{Q,el}}$ and D_c can differ by an order of magnitude. The discussion of experimental data in terms of effective velocities v and l and the discussions of diffusion bounds [13, 68] should take these distinctions and the influence of renormalization properly into account.

We find that \mathcal{L} depends strongly on T and that the WF law is typically violated with \mathcal{L} being either larger or smaller than the Sommerfeld value $\pi^2/3$ in several regimes even by a factor of ~ 2 . All these deviations bring a clear message: the usual practice of estimating κ_{el} using the WF law is problematic.

The temperatures of our FTLM simulations are well above the experimental ones, yet it is interesting to note the different status of the Mott-insulating case where the much larger experimental thermal conductiv-

ity points to a very rapid growth of l with lowering T . Conversely, in the doped case the measured κ_{el} has similar values as the Hubbard model result at much higher temperatures, suggesting that κ_{el} is only weakly temperature dependent in between.

We explore lower temperatures within the DMFT approximation and indeed find such behavior. We also present results obtained with a phenomenological AMFL model and give predictions for κ_{el} and the Lorenz ratio for the overdoped cuprates in the temperature regime of experiments (see Appendix F).

For data availability, see Ref. 69.

ACKNOWLEDGMENTS

This work was supported by the Slovenian Research Agency (ARRS) under Program No. P1-0044. Part of computation was performed on the supercomputer Vega at the Institute of Information Science (IZUM) in Maribor.

Appendix A: Details of the FTLM calculations

The transport coefficients are defined via

$$j_n = -L_{11}\nabla\mu - L_{12}\nabla T/T, \quad (\text{A1})$$

$$j_Q = -L_{21}\nabla\mu - L_{22}\nabla T/T. \quad (\text{A2})$$

Here $L_{11} = \sigma_{n,n}$, $L_{12} = \sigma_{n,Q} = L_{21}$, $L_{22} = \sigma_{Q,Q}$ are conductivities which are obtained by zero frequency limit ($\omega = 0$) of the generalized conductivities at finite frequency ω [70]. These are calculated via the generalized susceptibility

$$\sigma_{A,B}(\omega) = \frac{\chi''_{A,B}(\omega)}{\omega}, \quad (\text{A3})$$

$$\chi_{A,B}(\omega) = \frac{i}{NV_{u.c.}} \int_0^\infty dt e^{i\omega t} \langle [\hat{J}_A(t), \hat{J}_B(0)] \rangle. \quad (\text{A4})$$

\hat{J}_A and \hat{J}_B are the current operators, associated with (conserved) quantities \hat{A} and \hat{B} , which can be derived from polarisation

$$\hat{P}_A = \sum_j x_j \hat{A}_j, \quad \hat{J}_A = \frac{d\hat{P}_A}{dt} = i[\hat{H}, \hat{P}_A]. \quad (\text{A5})$$

For the single band Hubbard model, the operators for particle and heat currents in x direction are given by

$$\hat{J}_n = -it \sum_{j,\sigma,\delta} R_\delta^x c_{j+\delta,\sigma}^\dagger c_{j,\sigma}, \quad (\text{A6})$$

$$\begin{aligned} \hat{J}_E = & -\frac{it^2}{2} \sum_{j,\sigma,\delta,\delta'} R_{\delta\delta'}^x c_{j+\delta+\delta',\sigma}^\dagger c_{j,\sigma} \\ & + \frac{itU}{2} \sum_{j,\sigma,\delta} R_\delta^x c_{j+\delta,\sigma}^\dagger c_{j,\sigma} (n_{j+\delta,\bar{\sigma}} + n_{j,\bar{\sigma}}), \end{aligned} \quad (\text{A7})$$

$$\hat{J}_Q = \hat{J}_E - \mu \hat{J}_n, \quad (\text{A8})$$

where $R_\delta^x = x_{j+\delta} - x_j$ and $R_{\delta\delta'}^x = x_{j+\delta+\delta'} - x_j$.

We also consider the 2D Heisenberg model with nearest neighbor interaction

$$\hat{H} = J \sum_{\langle ij \rangle} \hat{\mathbf{S}}_i \cdot \hat{\mathbf{S}}_j = \sum_i \hat{H}_i, \quad \hat{H}_i = J \hat{\mathbf{S}}_i \cdot (\hat{\mathbf{S}}_{i+1_x} + \hat{\mathbf{S}}_{i+1_y}), \quad (\text{A9})$$

where the sum runs over sites i on the square lattice. The energy current operator for the Heisenberg model reads

$$\begin{aligned} \hat{J}_E = & -iJ^2 \sum_i [\hat{O}_{i-1_x, i, i+1_x} + \hat{O}_{i-1_x, i, i+1_y} \\ & + \hat{O}_{i-1_x, i, i-1_y}], \end{aligned} \quad (\text{A10})$$

$$\hat{O}_{ijl} = \frac{1}{2} [\hat{S}_i^z \hat{S}_{jl}^\pm + \hat{S}_j^z \hat{S}_{li}^\pm + \hat{S}_l^z \hat{S}_{ij}^\pm], \quad (\text{A11})$$

$$\hat{S}_{jl}^\pm = \hat{S}_j^+ \hat{S}_l^- - \hat{S}_l^+ \hat{S}_j^-. \quad (\text{A12})$$

The spectra of dynamical quantities on finite clusters consist of δ functions which we broaden using a Gaussian kernel. Finite size effects at low- T manifest also as a growing contribution of the δ function at $\omega = 0$. We can thus use this as a criterion to estimate the lowest temperature at which we can trust our FTLM results and set the maximum acceptable fraction of the total spectra contained in $\delta(0)$ to $\lesssim 0.5\%$.

At the particle-hole symmetric point at half filling in the Hubbard model, L_{12} vanishes. Thus, $\sigma_{n,E} = \mu \sigma_{n,n}$ and $\kappa_{el} = (\sigma_{E,E} - \mu^2 \sigma_{n,n})/T$ with $\mu = U/2$. Where $\sigma_{n,n}$ has a charge gap and is exponentially suppressed (at temperatures in the Heisenberg regime), only $\sigma_{E,E}$ contributes to κ_{el} .

Appendix B: Cluster size and shape dependence for the Heisenberg model

Here we discuss in more detail the Heisenberg model results and in particular the possibility of κ_{el} having a peak at $T \sim 0.6J$ where c_{el} shows a peak. In Fig. 9 we show κ_{el} , c_{el} and $D_{Q,el}$ for several cluster sizes and shapes. The results for κ_{el} for square lattices show clear finite size effect at $T \lesssim 0.6J$. Although the results for

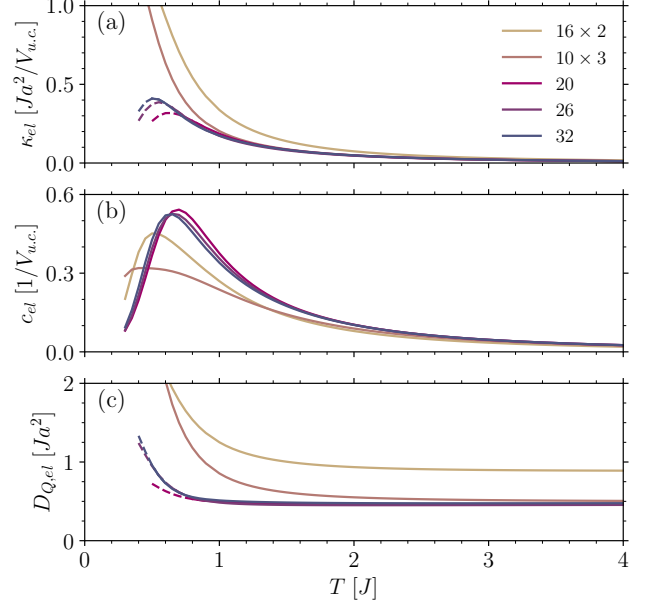


FIG. 9. Heat conductivity, specific heat and heat diffusion constant for different geometries in the Heisenberg model. We consider 2 and 3 rung ladders (labeled 16×2 and 10×3 , respectively) with periodic boundary conditions also in the transverse direction. 2d lattices with 20, 26 and 32 sites are tilted to allow unfrustrated antiferromagnetic correlations. Where finite-size effects are significant, we show the data dashed.

κ_{el} on square clusters do show a maximum corresponding to the maximum in c_{el} , the system size dependence at the maximum is still considerable and thus we cannot exclude the absence of the maximum in the thermodynamic limit. I.e., the mean free path becomes too large at low T making the finite-size effect too large to discriminate between a peak or a shoulder in κ_{el} . For comparison we also investigated κ_{el} for 2 leg and 3 leg ladders. These show a much stronger increase of $D_{Q,el}$ with decreasing T and therefore much more coherent behavior for $T \lesssim J$. Even in these long systems, we cannot conclusively determine the existence of a peak in κ_{el} at T where c_{el} has the peak, again due to finite size effect and long mean free paths. However, due to the strong increase of the mean free path with decreasing T , the absence of the peak and appearance of a shoulder is more likely. The “spin wave” result in Fig. 1 in the main text supports this scenario. It is also worth mentioning that the materials with 2 leg ladders are one of the best thermal conductors [27] despite having a spin gap of $\Delta_s \sim 0.5J$ [71].

Appendix C: Frequency spectra

The temperature evolution of optical spectra of $\kappa_{\text{el}}(\omega)$ and $\sigma_c(\omega)$ is shown on Fig. 10. One sees a Drude-like peak at low ω and a Hubbard satellite peak at $\omega \sim U$ with the two separated by a gap, which is most pronounced in $\sigma_c(\omega)$ at low T . $\sigma_c(\omega)$ clearly exhibits a gap and the weight of the Drude peak raises as T is increased. In the high T limit, the weight of this peak is comparable to the satellite peak. In contrast, $\kappa_{\text{el}}(\omega)$ does not show a clear gap or gap edge. In addition, the satellite peak is significantly smaller than the Drude peak at elevated T . This decrease in the relative weights of the two peaks originates in the difference of frequency dependence of $\sigma_{\text{E,E}}(\omega)$ and $\sigma_c(\omega)$.

FtLM results agree well with those from DQMC in particular at higher T . FtLM has a sharper Drude peak which deviates from a simple Lorentz shape. Because of this, FtLM also gives somewhat higher dc values for κ_{el} than DQMC.

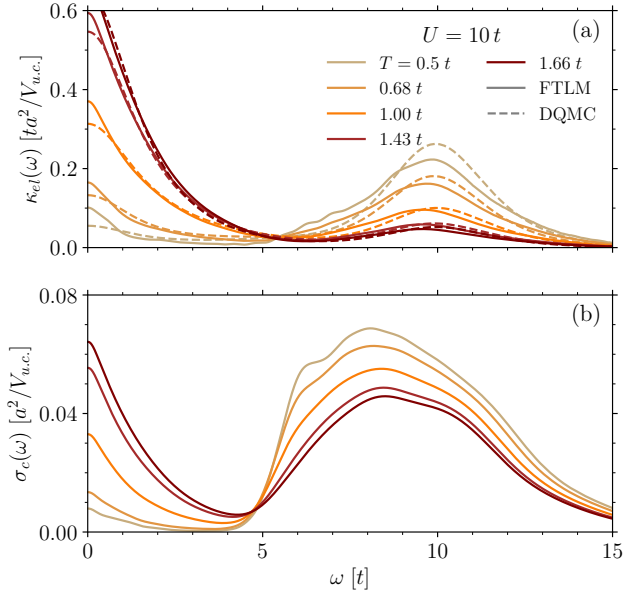


FIG. 10. The spectra $\kappa_{\text{el}}(\omega)$ and $\sigma(\omega)$ at different temperatures for $U = 10t$ and at half filling. DQMC results are taken from Ref. 29.

Appendix D: Vertex corrections

Recent investigations [7, 8] have tested the approximations of using local a self-energy and neglecting vertex corrections for calculation of dc charge conductivity σ_c . It was realized that the vertex corrections are substantial in the whole T regime. However, κ_{el} was not con-

sidered and we show in Fig. 11 κ_{el} as a function of temperature and frequency as calculated with FtLM and DMFT. DMFT approximates self energy with a local quantity and neglects the vertex corrections. For both, σ_c and κ_{el} , DMFT underestimates the DC conductivity as is shown in Fig. 11a, with the difference $\sim 50\%$ for both σ_c and κ_{el} . From this, one can say that the vertex corrections are substantial also for κ_{el} and that they have similar magnitude than for σ_c . Regarding the frequency dependence (see Fig. 11b), the inclusion of vertex corrections makes the low- ω (Drude) peak narrower.

However, both calculations point to the existence of a third peak in $\kappa_{\text{el}}(\omega)$ at $\omega \sim U/2$. Such a peak appears below $T \sim 1.7t$. We attribute this to the frequency dependence of $L_{12}(\omega)$, which has a zero at $\omega \sim U/2$. Thus, the frequency dependent Seebeck coefficient vanishes and heat transport is no longer suppressed by the term $L_{12}^2/(TL_{11})$ in Eq. 2. This leads to the peak in $\kappa_{\text{el}}(\omega \sim U/2)$. Such term and therefore the suppression can be traced back to the boundary condition of $j_n = 0$ leading to a buildup of charges on sample edges.

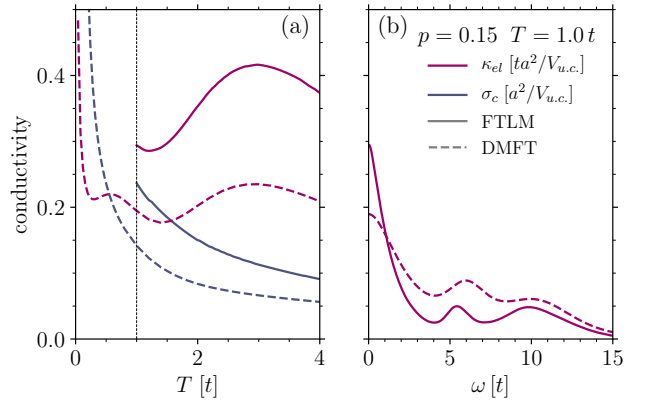


FIG. 11. Comparison of FtLM (solid) and DMFT (dashed lines) results for charge and heat conductivities as a function of temperature (a) and frequency (b) for the Hubbard model with $U = 10t$ and doping $p = 0.15$. The frequency dependence is shown for the lowest considered temperature $T = t$ and denoted with a dashed line in panel (a).

Appendix E: Diffusion constant with particle properties in the quasiparticle regime

Here we start with the bubble expressions for thermal conductivity κ_{el} and charge conductivity σ_{c} ,

$$\kappa_{\text{el}} = \frac{1}{T} \int d\omega \left(-\frac{\partial n_{\text{F}}}{\partial \omega}\right) \omega^2 \frac{2\pi}{V} \sum_k v_{0,k,x}^2 [A(k, \omega)]^2, \quad (\text{E1})$$

$$\sigma_{\text{c}} = \int d\omega \left(-\frac{\partial n_{\text{F}}}{\partial \omega}\right) \frac{2\pi}{V} \sum_k v_{0,k,x}^2 [A(k, \omega)]^2, \quad (\text{E2})$$

and rewrite them after some manipulation and use of approximations in terms of a quasiparticle properties, e.g. velocity, self-energy, density and renormalization. n_{F} is the ω dependent Fermi function, $v_{0,k,x}$ is the x component of bare band velocity at k point in the Brillouin zone, and $A(k, \omega)$ is the spectral function.

Using the isotropic property of the square lattice one can replace $v_{0,k,x}^2 \rightarrow v_{0,k}^2/2$. Further, one can use the velocity (or average velocity) at a certain energy to replace $v_{0,k}^2 \rightarrow v_{\epsilon}^2$ and if one neglects k dependence of self energy so that $A(k, \omega)$ is just a function of $\epsilon = \epsilon_k - \mu$ (and ω) one can write

$$\frac{2\pi}{V} \sum_k \frac{v_{0,k}^2}{2} [A(k, \omega)]^2 = \pi \int d\epsilon g_0(\epsilon) \frac{v_{\epsilon}^2}{2} [A(\epsilon, \omega)]^2. \quad (\text{E3})$$

Here noninteracting density of states $g_0(\epsilon) = (2/V) \sum_k \delta(\epsilon_k - \mu - \epsilon)$ is introduced. Assuming that $g_0(\epsilon)$ and v_{ϵ}^2 can be in the low T regime replaced by constants and with the values at the Fermi energy, namely $g_0(\epsilon_{\text{F}})$ and $v_{0,\text{F}}^2$, than the integral over ϵ can be performed.

$$\int d\epsilon [A(\epsilon, \omega)]^2 = \frac{1}{-2\pi\Sigma''(\omega)}. \quad (\text{E4})$$

This leads to the following expressions for the conductivities.

$$\kappa_{\text{el}} = \frac{1}{T} \int d\omega \left(-\frac{\partial n_{\text{F}}}{\partial \omega}\right) \omega^2 g_0(\epsilon_{\text{F}}) \frac{v_{0,\text{F}}^2}{-4\Sigma''(\omega)}, \quad (\text{E5})$$

$$\sigma_{\text{c}} = \int d\omega \left(-\frac{\partial n_{\text{F}}}{\partial \omega}\right) g_0(\epsilon_{\text{F}}) \frac{v_{0,\text{F}}^2}{-4\Sigma''(\omega)}. \quad (\text{E6})$$

Here $v_{0,\text{F}}$ is the bare Fermi velocity. At low T the Fermi function derivative filters out only low ω and we can roughly approximate the imaginary part of self energy with a constant, $\Sigma''(\omega) \sim \Sigma''(0)$. The integral over ω can than be performed, which leads to

$$\kappa_{\text{el}} = \frac{\pi^2}{3} g_0(\epsilon_{\text{F}}) T \frac{v_{0,\text{F}}^2}{-4\Sigma''(0)}, \quad (\text{E7})$$

$$\sigma_{\text{c}} = g_0(\epsilon_{\text{F}}) \frac{v_{0,\text{F}}^2}{-4\Sigma''(0)}. \quad (\text{E8})$$

This nicely demonstrates that κ_{el} and σ_{c} are given in terms of non-renormalized quantities like bare band density of states at Fermi energy $g_0(\epsilon_{\text{F}})$, bare Fermi velocity $v_{0,\text{F}}$ and bare particle scattering rate $\Gamma = -2\Sigma''(0)$. Here $\Sigma''(0)$ is imaginary part of self energy at $\omega = 0$.

Above equations also indicate which terms are related to static thermodynamic properties like c_{el} and χ_{c} and which to the diffusion constants. Note however, that these expression do not depend on the renormalization z , while c_{el} and χ_{c} do. See main text for further discussion.

By calculating the Lorenz ratio \mathcal{L} (Eq. 9) from Eqs. E7 and E8 one obtains the Sommerfeld value, $\mathcal{L} = \pi^2/3$. Note however, that here the ω dependence of $\Sigma''(\omega)$ was neglected and as discussed in the main text, ω dependence of $\Sigma''(\omega)$ effectively changes $\Sigma''(0)$ to $\Sigma''(\omega = 3T)$ in expression for κ_{el} (Eq. E7). This moves \mathcal{L} away from $\pi^2/3$ and therefore $\mathcal{L} = \pi^2/3$ only for the ω -independent scattering rate.

Appendix F: Anisotropic marginal Fermi liquid model for overdoped cuprates

1. Thermal conductivity of Tl2201

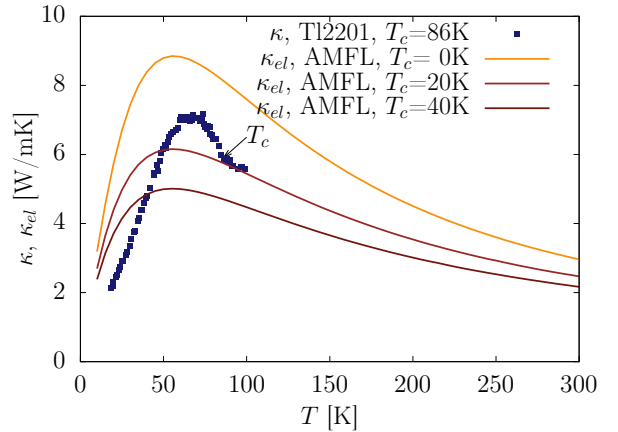


FIG. 12. Comparison of measured total κ for Tl2201 with $T_{\text{c}} = 86$ K [20, 72], with calculated electronic κ_{el} within AMFL model [34, 35] for $T_{\text{c}} = 0$ K, 20 K and 40 K on the highly overdoped side.

It is instructive to estimate also the electronic contribution to κ within the phenomenological approach in the measured temperature regime. For that we employ the anisotropic marginal Fermi liquid (AMFL) model [34, 35], which was devised from the angle-dependent magnetoresistance experiments [73–75] on overdoped $\text{Tl}_2\text{Ba}_2\text{CuO}_{6+\delta}$ (Tl2201) and quantitatively describes

the elastic impurity scattering, the isotropic Fermi-liquid-like scattering, and the anisotropic marginal-Fermi-liquid-like scattering. The AMFL model captures the specific heat, mass renormalization and ARPES experiments [34], as well as resistivity, optical conductivity, magnetoresistance and Hall coefficient [35] in Tl2201. We use the same parameters for the AMFL model as in Ref. 35 and show results for κ_{el} in Fig. 12. The results are obtained within the bubble approximation (Eq. E1) and are calculated for several dopings on the overdoped side, indicated by the values of the corresponding superconducting transition temperature T_c (0 K, 20 K and 40 K). The scattering rate becomes larger and more linear in T and ω as one reduces doping towards the optimal doping. Therefore, κ_{el} becomes smaller and also more constant in T (since $c_{el} \propto T$ and $D_{Q,el}$ approaches $1/T$ behavior). The AMFL results also show a maximum at $T \sim 50$ K since $D_{Q,el}$ saturates at the lowest T due to elastic impurity scattering while c_{el} is decreasing with decreasing T . This is an example of the low- T peak in κ_{el} due to saturation of l . Note that no superconducting effects are captured within the AMFL model. The results are compared to the total κ as measured in Tl2201 [72, 76]. Unfortunately, experimental data are available only close to optimal doping with $T_c = 86$ K (where AMFL is less valid) and report only total κ . It would be interesting to test the AMFL predictions for κ_{el} of Fig. 12 in the highly overdoped regime.

2. The Lorenz ratio in YBCO

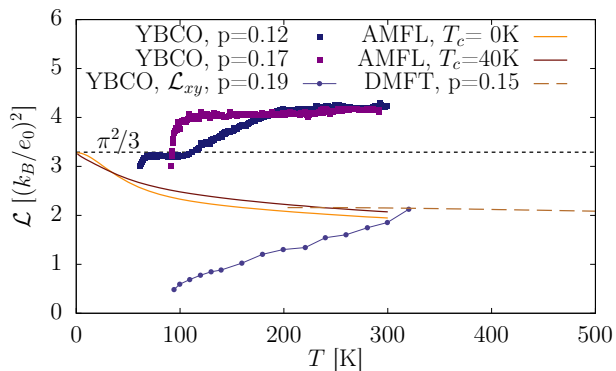


FIG. 13. Comparison of several measured data for Lorenz ratio \mathcal{L} for YBCO (taken from Ref. 16 and 64), with theoretical estimates from an AMFL model for overdoped cuprates [34, 35] and with DMFT calculation.

In Fig. 13 we show theoretical estimates for the Lorenz ratio from the AMFL model and the DMFT result. The AMFL results tend to the Sommerfeld value as $T \rightarrow 0$ due to elastic impurity scattering being dominant at lowest T . On a closer look, one sees that the AMFL model results for $T_c = 0$ K (only Fermi liquid like scattering) approaches Sommerfeld value quadratically in T while the AMFL result for $T_c = 40$ K (with considerable marginal Fermi liquid component in the scattering) approaches Sommerfeld value more linearly in T . \mathcal{L} therefore holds also information of the ω dependence of the scattering rate. See also Ref. 77 for further discussion of the T -dependence of \mathcal{L} at low T .

We show in Fig. 13 also the measured data for YBCO with doping $p=0.12$ and $p=0.17$. These are taken from Ref. 64 and differ from the complementary \mathcal{L}_{xy} measured data for YBCO with $p=0.19$ taken from Ref. 16. All measured data deviate from the standard theoretical expectations, which calls for further investigation.

We note that values of \mathcal{L} below the Sommerfeld value can arise also due to phonon scattering [19] or increased importance of normal vs. umklapp scattering [16].

[1] R. W. Hill, C. Proust, L. Taillefer, P. Fournier, and R. L. Greene, *Nature* **414**, 711 (2001).

[2] M. Yamashita, N. Nakata, Y. Senshu, M. Nagata, H. M.

- Yamamoto, R. Kato, T. Shibauchi, and Y. Matsuda, *Science* **328**, 1246 (2010).
- [3] S. Lee, K. Hippalgaonkar, F. Yang, J. Hong, C. Ko, J. Suh, K. Liu, K. Wang, J. J. Urban, X. Zhang, C. Dames, S. A. Hartnoll, O. Delaire, and J. Wu, *Science* **355**, 371 (2017).
- [4] P. T. Brown, D. Mitra, E. Guardado-Sanchez, R. Nourafkan, A. Reymbaut, C.-D. Hébert, S. Bergeron, A.-M. S. Tremblay, J. Kokalj, D. A. Huse, P. Schauf, and W. S. Bakr, *Science* **363**, 379 (2019).
- [5] J. Kokalj, *Phys. Rev. B* **95**, 041110 (2017).
- [6] E. Perepelitsky, A. Galatas, J. Mravlje, R. Žitko, E. Khatami, B. S. Shastry, and A. Georges, *Phys. Rev. B* **94**, 235115 (2016).
- [7] J. Vučičević, J. Kokalj, R. Žitko, N. Wentzell, D. Tanasković, and J. Mravlje, *Phys. Rev. Lett.* **123**, 036601 (2019).
- [8] A. Vranić, J. Vučičević, J. Kokalj, J. Skolimowski, R. Žitko, J. Mravlje, and D. Tanasković, *Phys. Rev. B* **102**, 115142 (2020).
- [9] E. W. Huang, R. Sheppard, B. Moritz, and T. P. Devereaux, *Science* **366**, 987 (2019).
- [10] O. Gunnarsson, M. Calandra, and J. E. Han, *Rev. Mod. Phys.* **75**, 1085 (2003).
- [11] M. A. Nichols, L. W. Cheuk, M. Okan, T. R. Hartke, E. Mendez, T. Senthil, E. Khatami, H. Zhang, and M. W. Zwierlein, *Science* **363**, 383 (2019).
- [12] M. Ulaga, J. Mravlje, and J. Kokalj, *Phys. Rev. B* **103**, 155123 (2021).
- [13] J. Zhang, E. M. Levenson-Falk, B. J. Ramshaw, D. A. Bonn, R. Liang, W. N. Hardy, S. A. Hartnoll, and A. Kapitulnik, *Proc. Natl. Acad. Sci.* **114**, 5378 (2017).
- [14] J. Zhang, E. D. Kountz, E. M. Levenson-Falk, D. Song, R. L. Greene, and A. Kapitulnik, *Phys. Rev. B* **100**, 241114 (2019).
- [15] V. Martelli, J. L. Jiménez, M. Continentino, E. Baggio-Saitovitch, and K. Behnia, *Phys. Rev. Lett.* **120**, 125901 (2018).
- [16] Y. Zhang, N. P. Ong, Z. A. Xu, K. Krishana, R. Gagnon, and L. Taillefer, *Phys. Rev. Lett.* **84**, 2219 (2000).
- [17] K.-S. Kim and C. Pépin, *Phys. Rev. Lett.* **102**, 156404 (2009).
- [18] R. Mahajan, M. Barkeshli, and S. A. Hartnoll, *Phys. Rev. B* **88**, 125107 (2013).
- [19] A. Lavasani, D. Bulmash, and S. D. Sarma, *Phys. Rev. B* **99**, 085104 (2019).
- [20] R. C. Yu, M. B. Salamon, J. P. Lu, and W. C. Lee, *Phys. Rev. Lett.* **69**, 1431 (1992).
- [21] P. B. Allen, X. Du, L. Mihaly, and L. Forro, *Phys. Rev. B* **49**, 9073 (1994).
- [22] J.-Q. Yan, J.-S. Zhou, and J. B. Goodenough, *New J. Sci.* **6**, 143 (2004).
- [23] C. Hess, B. Büchner, U. Ammerahl, L. Colonescu, F. Heidrich-Meisner, W. Brenig, and A. Revcolevschi, *Phys. Rev. Lett.* **90**, 197002 (2003).
- [24] C. H. Mousatov and S. A. Hartnoll, *Nat. Phys.* **16**, 579 (2020).
- [25] X. Zotos, *Phys. Rev. Lett.* **82**, 1764 (1999).
- [26] X. Zotos, *J. Phys. Soc. Japan* **74**, 173 (2005).
- [27] C. Hess, *Eur. Phys. J. Spec. Top.* **151**, 73 (2007).
- [28] C. Karrasch, *New J. Phys.* **19**, 033027 (2017).
- [29] W. O. Wang, J. K. Ding, B. Moritz, E. W. Huang, and T. P. Devereaux, *Phys. Rev. B* **105**, L161103 (2022).
- [30] T. G. Kiely and E. J. Mueller, *Phys. Rev. B* **104**, 165143 (2021).
- [31] U. Schneider, L. Hackermüller, J. P. Ronzheimer, S. Will, S. Braun, T. Best, I. Bloch, E. Demler, S. Mandt, D. Rasch, and A. Rosch, *Nat. Phys.* **8**, 213 (2012).
- [32] E. Guardado-Sanchez, A. Morningstar, B. M. Spar, P. T. Brown, D. A. Huse, and W. S. Bakr, *Phys. Rev. X* **10**, 011042 (2020).
- [33] J. Mravlje, M. Ulaga, and J. Kokalj, *Phys. Rev. Research* **4**, 023197 (2022).
- [34] J. Kokalj and R. H. McKenzie, *Phys. Rev. Lett.* **107**, 147001 (2011).
- [35] J. Kokalj, N. E. Hussey, and R. H. McKenzie, *Phys. Rev. B* **86**, 045132 (2012).
- [36] J. Jaklič and P. Prelovšek, *Adv. Phys.* **49**, 1 (2000).
- [37] P. Prelovšek and J. Bonča, *Strongly Correlated Systems: Numerical Methods*, edited by A. Avella and F. Mancini, Springer Series in Solid-State Sciences (Springer Berlin Heidelberg, 2013).
- [38] J. Kokalj and R. H. McKenzie, *Phys. Rev. Lett.* **110**, 206402 (2013).
- [39] R. Žitko and T. Pruschke, *Phys. Rev. B* **79**, 085106 (2009).
- [40] R. Žitko, “Nrg ljubljana,” (2021).
- [41] We use the specific heat at fixed density or doping, which is in contrast with the specific heat at fixed chemical potential calculated in Refs. 36, 38, and 43.
- [42] P. Prelovšek, J. Kokalj, Z. Lenarčič, and R. H. McKenzie, *Phys. Rev. B* **92**, 235155 (2015).
- [43] J. Bonča and P. Prelovšek, *Phys. Rev. B* **67**, 085103 (2003).
- [44] H. Eskes, A. M. Oleś, M. B. J. Meinders, and W. Stephan, *Phys. Rev. B* **50**, 17980 (1994).
- [45] M. Hofmann, T. Lorenz, K. Berggold, M. Grüninger, A. Freimuth, G. Uhrig, and E. Brück, *Phys. Rev. B* **67**, 184502 (2003).
- [46] J. Schnack, J. Schulenburg, and J. Richter, *Phys. Rev. B* **98**, 094423 (2018).
- [47] P. Sengupta, A. W. Sandvik, and R. R. P. Singh, *Phys. Rev. B* **68**, 094423 (2003).
- [48] M. S. Makivić and H.-Q. Ding, *Phys. Rev. B* **43**, 3562 (1991).
- [49] S. Chakravarty, B. I. Halperin, and D. R. Nelson, *Phys. Rev. B* **39**, 2344 (1989).
- [50] J.-K. Kim and M. Troyer, *Phys. Rev. Lett.* **80**, 2705 (1998).
- [51] Average velocity is calculated as the expectation value $v = \int |\nabla_{\mathbf{k}} \epsilon_{\mathbf{k}}| n_{\mathbf{k}} d^2 k / \int n_{\mathbf{k}} d^2 k$, where $\epsilon_{\mathbf{k}} = 2J\sqrt{1 - \gamma_{\mathbf{k}}^2}$ is the magnon dispersion, $\gamma_{\mathbf{k}} = \frac{1}{2}(\cos(k_x) + \cos(k_y))$, and $n_{\mathbf{k}}$ is the Bose function.
- [52] J.-i. Igarashi and T. Nagao, *Phys. Rev. B* **72**, 014403 (2005).
- [53] J. Bonča and J. Jaklič, *Phys. Rev. B* **51**, 16083 (1995).
- [54] Obtained with similar estimate as the results for a MIR limit for electrical conductivity in Appendix in Ref. 10. The same estimate can be obtained also by using the Wiedemann-Franz law and the MIR limit for the charge conductivity.
- [55] X. Deng, J. Mravlje, R. Žitko, M. Ferrero, G. Kotliar, and A. Georges, *Phys. Rev. Lett.* **110**, 086401 (2013).

- [56] F. Krien, E. G. C. P. van Loon, M. I. Katsnelson, A. I. Lichtenstein, and M. Capone, *Phys. Rev. B* **99**, 245128 (2019).
- [57] N. Pakhira and R. H. McKenzie, *Phys. Rev. B* **91**, 075124 (2015).
- [58] Since on a square lattice the Fermi velocity is not constant over the Fermi surface the $v_{0,F}^2$ is replaced with its averaged over the Fermi surface value $v_{0,F}^2 = \int d^2k v_{0,k}^2 \delta(\epsilon_k - \epsilon_F) / \int d^2k \delta(\epsilon_k - \epsilon_F)$.
- [59] Since $(-\frac{\partial n_F}{\partial \omega})\omega^2$ mostly weights positive and negative frequencies $\omega \sim \pm 3T$ and in DMFT the $\Sigma''(\omega)$ is not particle-hole symmetric (even in ω), the value of $\Sigma''(\omega = 3T)$ should be understood as $\Sigma''(\omega = 3T) = [\Sigma''(3T) + \Sigma''(-3T)]/2$.
- [60] L. V. Pourovskii, J. Mravlje, A. Georges, S. I. Simak, and I. A. Abrikosov, *New J. Phys.* **19**, 073022 (2017).
- [61] The same dependencies are obtained by using constant diffusion constants and dependencies $\chi_c \propto 1/T$ and $c_{el} \propto 1/T^2$.
- [62] W. O. Wang, J. K. Ding, Y. Schattner, E. W. Huang, B. Moritz, and T. P. Devereaux, [arXiv:2208.09144](https://arxiv.org/abs/2208.09144) [cond-mat] (2022).
- [63] For LCO we used parameters $J = 1550$ K, lattice constants $a_0 = 3.8$ Å and $c_0 = 13.2$ Å [23] with two CuO planes within c_0 .
- [64] K. Takenaka, Y. Fukuzumi, K. Mizuhashi, S. Uchida, H. Asaoka, and H. Takei, *Phys. Rev. B* **56**, 5654 (1997).
- [65] For YBCO we used unit cell parameters $a_0 = 3.82$ Å, $b_0 = 3.89$ Å and $c_0 = 11.68$ Å from Ref. 78 and 79 together with $t = 0.3$ eV and two CuO planes within c_0 .
- [66] H. Minami, V. W. Wittorff, E. A. Yelland, J. R. Cooper, C. Changkang, and J. W. Hodby, *Phys. Rev. B* **68**, 220503 (2003).
- [67] A. Waske, C. Hess, B. Büchner, V. Hinkov, and C. Lin, *Phys. C: Supercond.* **460-462**, 746 (2007).
- [68] S. A. Hartnoll, *Nat. Phys.* **11**, 54 (2015).
- [69] The data and scripts needed to reproduce the figures can be found at: <https://doi.org/10.5281/zenodo.6985239>.
- [70] B. S. Shastry, *Rep. Prog. Phys.* **72**, 016501 (2008).
- [71] E. Dagotto, *Rep. Prog. Phys.* **62**, 1525 (1999).
- [72] F. Yu, M. Salamon, V. Kopylov, N. Kolesnikov, H. Duan, and A. Hermann, *Phys. C: Supercond.* **235-240**, 1489 (1994).
- [73] M. Abdel-Jawad, M. P. Kennett, L. Balicas, A. Carrington, A. P. Mackenzie, R. H. McKenzie, and N. E. Hussey, *Nat. Phys.* **2**, 821 (2006).
- [74] M. Abdel-Jawad, J. G. Analytis, L. Balicas, A. Carrington, J. P. H. Charmant, M. M. J. French, and N. E. Hussey, *Phys. Rev. Lett.* **99**, 107002 (2007).
- [75] M. M. J. French, J. G. Analytis, A. Carrington, L. Balicas, and N. E. Hussey, *New J. Phys.* **11**, 055057 (2009).
- [76] F. Yu, V. Kopylov, M. Salamon, N. Kolesnikov, M. Hubbard, H. Duan, and A. Hermann, *Phys. C: Supercond.* **267**, 308 (1996).
- [77] E. Tulipman and E. Berg, [arXiv:2211.00665](https://arxiv.org/abs/2211.00665) [cond-mat] (2022).
- [78] S. I. Bondarenko, V. P. Kovrya, A. V. Krevsun, and S. I. Link, *Low Temp. Phys.* **43**, 1125 (2017).
- [79] D. Varshney, A. Yogi, N. Dodiya, and I. Mansuri, *J. Mod. Phys.* **2**, 922 (2011).